Castration Model Illuminates Sex Differences in Healthy Aging: Insights from Metabolome and Transcriptome Analyses

Jianjun Jiang[1,2#], Na Ge[2], Yuzhi Wang[2], Juntao Qi[3], Guibiao Wen[3], Xiufen Gu[2], Xuewen Yu[4], Muming Shao[4], Yueming Luo[4], Kangshuyun Gu[2], Feng Lin[3], Shudong Yang[2#], Wei Wei [1#],

[1] Institute for Systems Biology, Seattle, USA;
[2] Department of Nephrology, [3] Department of Urology, [4] Department of Pathology, [5] Department of Geriatrics, Shenzhen Traditional Chinese Medicine Hospital, The Fourth Clinical Medical College of Guangzhou University of Chinese Medicine, Shenzhen, China;

Authors' e-mails:
Jianjun Jiang : jjiang@systemsbiology.org; Na Ge: gena.sz@gzucm.edu.cn;
Yuzhi Wang : wangyuzhi997@gmail.com; Juntao Qi: juntaoqi@outlook.com;
Guibiao Wen: guibiaowen@163.com; Xiufen Gu: nodo1007@163.com;
Xuewen Yu:yuxuewen365@163.com; Muming Shao: smm1320@gzucm.edu.cn;
Yueming Luo: yuemingluo@163.com; Kangshuyun Gu: gukangshuyun@foxmail.com;
Feng Lin: lf0237@gzucm.edu.cn;Shudong Yang: ysd0870@gzucm.edu.cn;
Wei Wei:wwei@systemsbiology.org;

[*] These authors contribute equally to this work
[#] Corresponding authors
Jianjun Jiang, Ph.D., E-mail: jjiang@systemsbiology.org
Shudong Yang: ysd0870@gzucm.edu.cn
Wei Wei, Ph.D., E-mail: wwei@systemsbiology.org;

Abstract

Females typically outlive males, a disparity mitigated by castration, yet the molecular underpinnings remain elusive. Our study leverages untargeted metabolomics and RNA sequencing to uncover the pivotal compounds and genes influencing healthy aging post-castration, examining serum, kidney, and liver biospecimens from 12-week and 18-month old castrated male mice and their unaltered counterparts. Behavioral tests and LC-MS/MS metabolomics reveal that castrated males exhibit altered steroid hormones, superior cognitive performance, and higher levels of anti-oxidative compounds like taurine, despite identical diets. Integrated metabolome-transcriptome analysis confirms reduced lipid peroxidation and oxidative stress in female and castrated male mice, suggesting a protective mechanism against aging. Histological examinations post-cisplatin treatment highlight the model's applicability in studying drug toxicity and reveal varying susceptibility in organ-specific toxicities, underlining the crucial role of sex hormones in physiological defenses. In essence, our castration model unveils a feminized metabolic and transcriptomic intermediary, serving as a robust tool for studying gender-specific aspects of healthy aging and exploring sex hormone-induced differences in diverse biomedical domains.

Key words: Sex difference; Sex hormones, Healthy aging, Castration model, Metabolomics, Transcriptome

INTRODUCTION

Sex-related differences in human are easy to find, where women consistently live longer than men [1]. In the longevous population - centenarians, women always outnumber men [2]. While past research have attributed longer female lifespans to healthier lifestyles, such as lower alcohol and tobacco consumption [2-4], a compiled demographic study of 134 mammal populations across 101 species revealed that females have a median lifespan that is on average 18.6% longer than their male counterparts. This suggests the intrinsic biological mechanisms underlie the sex differences in lifespan [1]. Sex hormones were considered as key factors in explaining the sex difference patterns of longevity [5]. Estrogen was proposed to play protective roles against many diseases, while testosterone may increase the risk of developing diseases and loss of testosterone perhaps promote healthy aging and longevity [6, 7]. Nevertheless, more evidence from clinical trials is needed to elucidate it.

Aging stands as a paramount risk factor for a myriad of chronic diseases, with differential impacts on males and females. The absence of a stable and broadly applicable model continues to pose a significant challenge in the quest to unravel the intricacies of sex differences in healthy aging [8]. In this study, we present castration as an effective model for understanding the sex-based differences in healthy aging. This is supported by a growing body of evidence demonstrating castration can extend the lifespan across multiple mammal species and decelerate intrinsic aging processes by slowing the DNA methylation clock [9]. For example, castration at prepubertal period can significantly prolong male mice lifespan, which eliminates the sex differences in lifespan and growth trajectories [10]. Castration in human, with statistical evidence shown that Korean eunuchs lived 14.4–19.1 years longer than normal men of similar socio-economic status [11]. However, the extent to which castration promotes healthy aging, and the underlying mechanisms, remain largely unexplored. Considered that genome sequences retain the same pre- and post-castration, we hypothesized that alterations in hormones spectrum and associated changes in metabolome, transcriptome and epigenome by castration possibly act as healthy aging regulators and affects lifespan extension. In this study, we utilized untargeted liquid chromatography with tandem mass spectrometry (LC-MS/MS) metabolomics and deep RNA sequencing (RNA-seq) to interrogate serum, kidney, and liver samples collected from 12 weeks and 18 months old male, female and castrated male mice to explore the versatile

84 perspectives of sex-related healthy aging mechanisms.

85

RESULTS

Castration is an effective model of healthy aging

To elucidate the effects of castration on lifespan extension and healthy aging, we employed multi-omics approaches to resolve the potential roles at both molecular and phenotypic levels (**Figure 1A)**. Young adult C57/BL6 mice were castrated at 8 weeks old (casM) and exhibited weight gain post-castration, but attained similar body weights as the sham males (shamM) by 60 weeks. This pattern align with findings in prepubertal castration models using UM-HET3 mice (**Figure 1B)** [10]**.** Hair graying, a common aging marker in both mice and humans [12], was notably delayed in casM compared to shamM at 13 months, indicating a more youthful phenotype in the castrated group (**Figure 1C**). Given the known correlation between ages 10 – 14 months in mice and 38 – 47 years in humans, where senescence-related changes become prominent [13], we conducted aging-related behavioral analyses. These included Barnes maze (BM), open field (OF) and novel object recognition (NOR) tasks to evaluate the spatial learning and memory, locomotor activity, and recognition memory in 12 – 13 month-old casM, shamM and sham female (shamF) mice. Previous studies have shown pronounced cognitive decline in middle-aged mice (8 – 12 months) as assessed by the BM test [14]. However, our results showed that middle-aged casM demonstrated superior performance, spending less time and making fewer errors with less immobile time in locating the escape hole than shamM and/or shamF (**Figure 1D-F**), hinting at a mitigated cognitive decline in casM (**Figure 1E-F**). Non-significant difference was found in OF and NOR tasks across the three groups (**Supplementary Figure 1**). More than possessing longer lifespans, our results revealed that castration confers a protective effect against cognitive decline. This selective enhancement in spatial learning and memory may reflect the differential influence of castration on brain regions, particularly affecting areas like the hippocampus that are crucial for navigation tasks, while exerting less impact on regions involved in locomotor and recognition memory functions.

Castration affected the secretion of steroid hormone spectrum

Hormones, serving as vital chemical messengers, travel through from bloodstream to tissues for coordinating a range of biological functions, with their dysregulation impacting development [15], aging [16] and disease progression [17]. The effect of surgical castration, specifically the removal of the testes, leads to a marked reduction

in testosterone (TS) levels. However, the broader hormone changes resulting from castration remain underexplored. Here, we employed ultra-high-performance liquid chromatography coupled with multiple reaction monitoring tandem mass spectrometry (UHPLC-MRM-MS/MS) to analyze 17 targeted steroid hormones (SHs) in the serum of casM, shamM and shamF mice, four weeks post-operation.

Given the limited volume of mouse serum available for SH measurement, we could only detect and compare 10 SH types across three groups. Notably, castration significantly altered SH secretion in casM (**Figure 2A**). As expected, testosterone and its more potent form, dihydrotestosterone, were remarkably reduced in CasM, to the point of being barely detectable (**Figure 2B-C**). Intriguingly, CasM mice exhibited a significant higher level of 17α-Hydroxyprogesterone (17α-OHP) (**Figure 2D**) and lower androstenedione (A4) compared to shamM ($p < 0.05$) (**Figure 2E**). These hormones, precursors to TS, might be part of a compensatory mechanism in response to TS deprivation [18]. In addition, we observed slight increases in aldosterone (ALD) and corticosterone (CORT) in casM, with p-values of 0.11 and 0.083, respectively (**Supplementary Figure 2**). ALD, a mineralocorticoid, and CORT, a glucocorticoid, are primarily produced by the adrenal cortex. Their upregulation may suggest an activated stress response and changes in mineral and glucose homeostasis consequent to TS deprivation.

To elucidate metabolites associated with TS, we conducted an untargeted metabolomics analysis by LC-MS/MS on serum samples from three groups of mice, four weeks post-operation. A total of 1495 compounds with MS^2 scores ≥ 0.3 were identified. Notably, coexpression analysis revealed that 17 of these compounds, which include 11 bioactive lipids, showed a significant correlation with TS levels ($|r| \geq 0.8$, $p \leq 0.001$, **Figure 2F**), These 11 lipids encompass a range of molecules such as prostaglandin B2 (PGD2), a specific phosphatidylcholine (PC) variant, lysophosphatidylserine (LPS), lysophosphatidic acid (LPA), cyclic PA (CPA), glucuronosyldiacylglycerol (GlcADG), sulfurHexosylceramide (SHexCer), and four types of ceramide fatty acids (Cer) (**Supplementary Table 1**). While further investigation is required to solidify these findings, our coexpression analysis suggests that TS deprivation may significantly influence peripheral lipid metabolism, particularly impacting ceramide and lysophosphatide pathways.

Characterization of sex-related serum metabolomic features

To assess the serum metabolomic profile differences among shamM, shamF, and CasM mice at 12 weeks old (12w, 4 weeks post sham/castration procedures), principal component analysis (PCA) was performed using data from 1495 compounds identified by LC-MS/MS (**Figure 3A**). Lipid and lipid-like molecules constituted the largest category (~33%) of these compounds (Figure 3B). A comparison of shamM and shamF groups to explore sex-specific differences in serum metabolic activity revealed 255 significantly altered metabolites (SAMs) were identified (**Supplementary Table 2**), with the top SAMs (ranked by fold changes) displayed in **Supplementary Figure 3A.** Despite all mice receiving the same diet, we observed notably higher levels of antioxidants and anti-inflammatory compounds in shamF compared to shamM. These compounds, likely derive from food intake, included carnosic acid [19], arachidonic acid [20], choline [21], nicotinamide [22], D-pantothenic acid [23], gamma-crocetin [24], ruscogenin [25], 4-hydroxycinnamic acid [26], oleamide [27, 28] (**Figure 3C).** Conversely, shamM mice exhibited elevated levels of metabolites associated with resistance to high-fat diet-related diseases, such as 5-HEPE [29] and 12-HEPE [30], and a higher level of protective L-Anserine [31] than shamF (**Figure 3C)**. Consistently, obesity-related compounds such as LysoPE(0:0/20:3(11Z,14Z,17Z)/0:0) (LysoPE) [32] and 7−Ketocholesterol (7-KC) [33] were found to be lower in male (**Figure 3C)**, offering insights into why obesity is more prevalent in women than men [34].

Differential abundance (DS) score of the 255 SAMs was calculated to inform the overall changes of each pathway (Figure 3D). These SAMs were found to be highly enriched in lipid metabolism related pathways such as “sphingolipid signaling pathway”, “regulation of lipolysis in adipocytes” and “arachidonic acid metabolism”, suggesting a sex dimorphism in lipid metabolism. Additionally, a serum untargeted metabolomic analysis in the same groups at 18 months old identified 868 compounds, with “lipid and lipid-like molecules” again being the predominant category” (**Supplementary Figure 3B**). PCA analysis suggested that the metabolic profile of 18-month-old casM mice closely resembled that of shamF (**Supplementary Figure 3C**). Similar to the younger mice, older shamF demonstrated higher levels of protective compounds derived from the same diet compared to shamM **(Figure S3D, Supplementary Table 3**), suggesting a potentially stronger ability in females to generate healthy compounds from the same chow.

Metabolomic feminization and taurine enrichment in castrated male mice

188 In our analysis of 12-week-old mice serum, a comparative study between casM and
189 shamF mice identified 170 SAMs. In contrast, comparisons of "casM vs shamM" and
190 "shamF vs shamM" revealed 280 and 255 SAMs, respectively (**Figure 4A,**
191 **Supplementary Table 4**). Hierarchical Clustering of the 1495 identified compound
192 demonstrated a closer metabolic profile between casM and shamF than between casM
193 and shamM (**Figure 4B**). These findings, achieved without altering genetic background,
194 suggest that castration feminizes the metabolomic traits of male mice. When ranking
195 these SAMs by fold change (FC), notable differences were observed between shamM
196 and casM. The most significantly upregulated metabolite in casM was the unsaturated
197 fatty acid, PI (16:1/18:2), with $\log_2$FC of 13.14, while the most downregulated was
198 guanosine, with a $\log_2$FC of -6.79. CasM mice exhibited elevated levels of various
199 metabolites associated with healthy aging, anti-skin aging, and anti-inflammation, such
200 as ectoine [35], resolvin D2 [36], oleamide [27, 28], taurine [37], taurocholic acid [38],
201 taurodeoxycholic acid [39], nicotinamide [40], ascorbic acid (vitamin C) [41], D-
202 pantothenic acid (vitamin B5) [42, 43] and choline [44] (**Figure 4C**). Similar to shamF,
203 casM mice also showed an enrichment of anti-oxidative metabolites likely derived from
204 plant-based foods, including ganoderenic acid C [45], oleuropeic acid [46], fasciculol
205 C [47], graveoline [48] (**Figure 4C**).
206 Enrichment analysis of the 280 SAMs from the "casM *vs* shamM" comparison
207 categorized them into pathways such as "bile secretion", "vitamin digestion and
208 absorption", "HIF-1 signaling pathway", "pyrimidine metabolism", various fatty acid
209 metabolism pathways including "arachidonic acid metabolism" and "regulation of
210 lipolysis in adipocytes". (**Figure 4D**). Interestingly, lipid metabolism-related pathways
211 were consistently enriched in both the "casM vs shamM" and "shamF vs shamM"
212 comparisons, indicating a potential sensitivity of lipid metabolism to the levels of SHs.
213 To investigate the metabolomic changes particularly derived from castration,
214 union SAMs among 12w-old casM, shamM and shamF groups were further classified
215 by c-means fuzzy clustering **(Figure 4E**, **Supplementary Table 5**). This analysis
216 revealed that cluster1 metabolites were notably elevated in casM compared to both
217 shamM and shamF. Topology-based pathway enrichment analysis indicated that
218 cluster1 metabolites were significantly ($p < 0.05$) enriched in pathways like "primary
219 bile acid biosynthesis", "D-glutamine and D-glutamate metabolism", "taurine and
220 hypotaurine metabolism" among others (**Figure 4F**). Notably, taurine levels were
221 higher in shamF than in shamM, and castration further augmented taurine levels along

222 with two key components of the taurine and hypotaurine metabolism pathway:
223 taurodeoxycholic acid (TDCA) and taurocholic acid (TCA) (**Figure 4G**). However, in
224 18m-old mice, a higher level of taurine with no significant changes of TDAC and TCA
225 were observed in shamM compared to shamF and casM, (**Figure 4H**), suggesting an
226 age-related sex dimorphism of taurine concentrations in mice serum. Bile acids (BA)
227 are crucial for maintaining lipid homeostasis and have been recognized as significant
228 signaling molecules during aging process [48]. Given that the SAMs from both "casM
229 vs shamM" and "shamF vs shamM" comparisons were significantly enriched in lipid-
230 related metabolic pathways, and the primary function of taurine is the conjugation of
231 cholesterol into bile acids [49], our findings suggest a potential link between taurine
232 and the sex and/or SH-related differences in lipid metabolism. Taurine, along with
233 TDCA and TCA, serve as antioxidants and protective factors against many degenerative
234 diseases [50]. A recent study has demonstrated that blood taurine levels decline with
235 age, but intake of taurine supplement at middle age can extend the healthy lifespan of
236 mice and monkeys [37]. Considering the established longevity of females and castrated
237 males over unaltered males, our results imply that mice with elevated taurine levels at
238 younger ages may reap more significant benefits than those with higher levels at older
239 ages.
240

241 **Co-expression analysis across serum, livers and kidneys identifies potential**
242 **taurine-related regulators**

243 Kidney and liver are two major organs of organisms, the sex differences of renal and
244 hepatic function have been aware over years [51]. To elucidate the sex and age-related
245 regulatory networks in kidney and liver functions, we analyzed metabolome and
246 transcriptome of renal cortex and left liver lobe from three groups of mice at 12 week
247 (12w) and 18 months (18m) old. We detected an average of 899 compounds across both
248 tissues, with 121 compounds common among kidneys, livers and serum samples in both
249 age groups of sham, shamF, and casM mice (**Figure 5A** and **Supplementary Table 6**).
250 Coexpression analysis of these 121 commonly detected metabolites (CDMs) revealed
251 4 major clusters (**Figure 5B**). Metabolite Set Enrichment Analysis (MSEA) indicated
252 that Clusters 1, 2 and 3 are primarily involved in "Bile Acid Biosynthesis" and "Glycine
253 and Serine Metabolism" pathways (**Supplementary Figure 5A-C**). Notably, two
254 compounds known for their health-protective properties, taurine and alpha-linolenic
255 acid (ALA), were grouped in Cluster 4. They exhibited a strong correlation ($r > 0.75$, p

256 < 0.01) with adenosine, xanthosine, 1-palmitoylglycerophosphoinositol, L-tyrosine,
257 erythrulose, glycolic acid, PC-M5', pyruvic acid and 5 other lipids include LPC(15:0),
258 LPE(18:2), LPE(20:3), LPS(20:4), FAHFA(18:1/22:3) (**Figure 5C**), suggesting a
259 potential link between Cluster 4 compounds and healthy aging. A recent study has
260 demonstrated that taurine intake can attenuate lipid peroxidative stress (LPOS) and lipid
261 metabolism disorder in mice, evidenced by decreased levels of malondialdehyde
262 (MDA), a marker of LPOS [52]. Similarly, ALA, an omega-3 polyunsaturated fatty acid
263 derived from plants, has also been shown to markedly reduce oxidative stress and
264 increase the lifespan of *Caenorhabditis elegans* in a dose-dependent manner [53].
265 Considering the fact that a linoleic acid-rich diet increases hepatic taurine [54] and the
266 observed strong association (r = 0.934) between taurine and ALA across three sample
267 types from three mouse groups and at two age stages, these results collectively suggest
268 potential role for ALA in taurine-mediated antioxidant defense and lipid metabolism
269 processes.

270 Due to the limited range of lipids identifiable by KEGG compounds database,
271 Cluster 4 compounds were showing enrichment in a few terms include "glyoxylate and
272 dicarboxylate metabolism", "tyrosine metabolism" and others (**Figure 5D**).
273 Noteworthy, xanthosine and adenosine, two key components of "purine metabolism"
274 pathway, were strikingly co-expressed with taurine (r = 0.973 and 0.874, respectively,
275 **Figure 5C**). Dysregulated purine metabolism has been implicated in many aging-
276 related disorders such as Alzheimer's diseases [55] and age-associated lower urinary
277 tract dysfunctions [56]. Considering taurine's role in aging delay [9], we hypothesized
278 that its influence on lifespan extension might also be linked to xanthosine and
279 adenosine-mediated purine metabolism, though further evidence is required to
280 substantiate this.

281 Considering the significance of taurine in aging and healthy aging, co-expression
282 analysis and c-means clustering were applied to identify genes that positively associated
283 with taurine. A total of 51 genes, whose expression levels showed similar dynamic trend
284 with taurine across casM, shamM and shamF mice in kidney and liver tissues at both
285 12w and 18m ages, were identified (**Figure 5E-G**). Among these, 15 genes exhibited a
286 generally decrease in expression in 18m tissues than 12w, such as *Hdac5, Preb, Plk2,*
287 *Atxn2* and *Trit* (**Figure 5E**). Two key lipid metabolism genes, *Srebf1* and *Ppard* were
288 among the 51 taurine-associated genes. *Srebf1* encodes sterol regulatory element-
289 binding protein 1 (SREBP1), a critical transcription factor regulating lipogenes

290 involved in fatty acid and cholesterol biosynthesis [57]. *Ppard* encodes Peroxisome
291 proliferator-activated receptor-delta (PPAR-δ), a member of the PPAR group in the
292 nuclear receptor superfamily, known for its ligand-binding domains (LBD) that
293 interacts with a broad range of lipid and lipid-like molecules [58]. This includes
294 multiple types of polyunsaturated fatty acids, such as arachidonic and linoleic acid [58].
295 Both PPAR-δ and SREBP1 are also involved in retinoid X receptors/ Vitamin D
296 Receptor (RXR/VDR) pathway (**Supplementary Table 7**). Given previous research
297 showing that intestinal-specific deletion of VDR increased taurine levels [59], it is
298 posited that taurine may also be associated with PPAR-δ and SREBP1 involved
299 RXR/VDR pathway. Taken together, our results from both metabolomics and RNA-seq
300 analysis strongly suggest that taurine is a key regulator in lipid peroxidation and
301 metabolism, potentially playing a significant role in the process of healthy aging.
302

303 **Joint metabolomic-transcriptomic analysis reveals a stronger capacity of**
304 **defensing lipid peroxidation in female and castrated male**

305 From deep RNA-seq analysis, we identified differentially expressed genes (DEGs)
306 among casM, shamM and shamF groups in kidney and liver tissues (**Figure 6A-B,**
307 **Supplementary Table 6**). In the kidneys of 12w old mice, over 4500 DEGs were noted
308 in the comparisons of "shamF *vs* shamM" and "casM *vs* shamM," while only 987 genes
309 showed differential expression between shamF and casM. Interestingly, livers seemed
310 to be less affected by sex and/or the changes of SH levels than kidneys as only 2053
311 and 2533 DEGs were detected in "shamF *vs* shamM" and "casM *vs* shamM"
312 comparisons, respectively, in 12w-old mice, and 546 DEGs between shamF and casM.
313 Hierarchical clustering of RNA-seq data also revealed that the transcriptomic profiles
314 of casM samples more closely resembled those of shamF than shamM samples, with
315 the exception of 18m-old livers, suggesting a feminizing effect of castration that creates
316 a crossover zone between male and female transcriptomic profiles in both kidney and
317 liver (**Figure 6C**). However, the impact of sex and/or SH levels on transcriptomes,
318 pronounced at 4 weeks post-castration, appeared to diminish in 18-month-old mice. In
319 this older age group, the numbers of DEGs among the 3 groups were reduced, especially
320 the comparisons of shamM with casM. In 18-month-old kidneys and livers of "casM *vs*
321 shamM", it showed only 435 and 353 DEGs, respectively.
322 Mapping the DEGs onto mouse chromosomes, we found that DEGs in "shamF vs
323 shamM" and "casM vs shamM" from both 12w and 18m-old liver tissues were

324 significantly clustered to chr4B3 (FDR < 0.05). Of the 145 annotated genes in chr4B3,
325 46 belong to the Major Urinary Proteins (*Mup*) family, with 25 being pseudogenes.
326 Except for *Mup4* and *Mup5*, which were barely detectable, the other *Mup* family genes
327 in chr4B3 were almost completely silenced in casM and shamF livers, showing an
328 average log2FC = -5.57 (**Figure 6SA-B**). *Mup14*, *7*, *11*, and *1* were the top 4
329 differentially expressed *Mup* genes. It is known that *Mup* genes, predominantly
330 expressed in the liver, exhibit sexually dimorphic traits. Male mice typically excrete 2–
331 8 times more Mup protein in their urine compared to females [60]. Our results indicate
332 that the expression of *Mup* genes is influenced not only by sex genotypes but also by
333 testosterone levels.

334 To identify potential long-term salutary regulatory elements brought by sex and/or
335 castration at old age, we conducted a joint metabolomic-transcriptomic analysis. Here,
336 shamM mice, typically having a shorter liferspan, served as controls, while shamF and
337 casM mice, associated with healthier and longer lifespans, were the focus [61]. We
338 utilized the SAMs and DEGs from "shamF *vs* shamM" for the joint analysis to
339 investigate female-specific signatures; meanwhile, the joint metabolomic-
340 transcriptomic analysis was also performed using the SAMs and DEGs from "casM *vs*
341 shamM" for interpreting castration-specific features. In 18m-old kidneys, both shamF
342 and casM groups showed enrichment in KEGG programs related to "lysosome" and
343 "cholesterol metabolism" (**Supplementary Table 8-9**). In the liver of the same age
344 group, the significantly enriched KEGG pathways in the "casM vs shamM" comparison
345 are illustrated in **Figure 6D**. Notably, 20 terms, such as "linoleic acid metabolism",
346 "arachidonic acid metabolism", "retinol metabolism", "Jak-stat3 signaling" and
347 "glutathione metabolism" were consistent with those in the "shamF vs shamM"
348 comparison (terms marked by orange in **Figure 6D and 6E, , Supplementary Table**
349 **10-11**). These KEGG terms are known to play critical roles in lipid peroxidation.

350 To further validate these findings, we measured levels of malondialdehyde (MDA)
351 - a final product of polyunsaturated fatty acids peroxidation, in the three groups of mice.
352 Results indicated that shamF mice exhibited the lowest, while shamM mice had the
353 highest MDA levels in 18m-old livers, suggesting that females and castrated males
354 experience less lipid oxidation stress than their male counterparts (**Figure 6F**).
355 Additional oxidative stress markers, SOD1 and SOD2, were also tested and showed
356 similar trends to MDA among three groups (**Supplementary Figure 6C**). Taken
357 together, our analysis suggests a close association between lipid metabolism and sex

358 and SH levels. CasM and shamF mice are likely to absorb more health-beneficial
359 compounds from their diet and experience reduced lipid peroxidative stress, potentially
360 contributing to their longer lifespans.
361
362 **Evaluating sex-dependent cisplatin toxicity through castration models**
363 Drug-induced tissue toxicity presents a significant challenge in the clinical application
364 of anti-tumor drugs. Platinum-based drugs (PBDs), such as cisplatin, is the mainstay of
365 cancer therapy, with nearly half of all patients receiving chemotherapy treated with
366 PBDs [62]. However, the therapeutic application of these drugs is tempered by adverse
367 side effects, including nephrotoxicity and hepatotoxicity, including nephrotoxicity and
368 hepatotoxicity, which exhibit differential impacts between male and female patients
369 [63]. To evaluate the utility of the castration model in studying sex-dependent toxicity
370 studies, we treated 12w-old mice (4 weeks post-castration/sham procedure) with a low
371 dose of cisplatin twice, every 72 hours. It is well-established that the kidney, and to a
372 lesser extent the liver, are susceptible to cisplatin-induced damage. Consequently, we
373 harvested renal cortex and left liver lobe tissues post-treatment for histological analysis.
374 Hematoxylin and eosin (H&E) staining of liver tissues showed the most severe
375 liver injury in shamF mice, characterized by marked steatosis, sinusoidal congestion,
376 and hemorrhage. In contrast, sham-operated male (shamM) and castrated male (casM)
377 mice displayed comparatively less hepatic damage (**Figure 6G**). Conversely, Periodic
378 Acid Schiff (PAS) staining of kidney tissues showed that casM mice had more severe
379 kidney damages than both shamF and shamM, with a notable increase in acute renal
380 tubule injury (**Figure 6H**). Previous studies on cisplatin-induced hepatotoxicity have
381 yielded limited insights regarding sex differences. However, substantial evidence
382 indicates that males are more susceptible to cisplatin-induced nephrotoxicity [63].
383 Studies administering cisplatin to rats at both 2 weeks (1 mg/kg/day) and a single dose
384 (7.5 mg/kg) have shown that males experience more severe nephrotoxic effects than
385 females [64]. Our pathological observations, combined with previous findings and the
386 fact that castrated male (casM) mice have the lowest testosterone (TS) levels, suggest
387 that intermediate TS levels, similar to those in shamF mice, may offer greater protection
388 against renal toxicity induced by cisplatin.
389
390 **DISCUSSION**
391 The burgeoning aging population has become a global concern, poised to increase the

392 prevalence of age-related diseases [65]. Hence, it is imperative to gain a better
393 understanding of the regulatory factors contributing to healthy longevity. Historically,
394 sexual dimorphism in aging has been largely overlooked, despite the fact that females
395 consistently outlive males. While castration is a common practice in animal husbandry,
396 known to extend the lifespan of domesticated dogs and cats in veterinary medicine, its
397 implications for aging research have only recently been explored [66]. For instance,
398 castrated domestic sheep exhibit both extended lifespan and decelerated epigenetic
399 aging compared to their intact male counterparts [9]. Similarly, survival assays in
400 genetically diverse mice reveal that castration extends longevity, implicating post-
401 pubertal testicular actions as key determinants of sex differences in lifespan and growth
402 trajectories [10]. Moreover, castration has been shown to induce metabolic remodeling
403 in male hearts [67] and mitigate the formation of aging-induced abdominal aortic
404 aneurysms [68].

405 Nevertheless, the utility of castration as a model for studying sex differences in
406 healthy aging and the underlying molecular mechanisms remain underexplored. In this
407 study, we employed multi-omics approaches to systematically investigate sex
408 differences in lifespan at both young (12w) and old (18m) stages of mice. Intriguingly,
409 despite being fed the same diet, shamF and casM exhibited elevated levels of multiple
410 food-derived health-promoting compounds than shamM. Given the influential role of
411 gut microbiome in aging and its known sex-dependent modulation [69, 70], we
412 hypothesize that sex hormones may involve in the regulation the microbial community,
413 thereby affecting the bioavailability of these protective compounds from food.

414 Previous research has offered mixed insights into the impact of castration on
415 cognitive function. One such study employed a dual-task approach – utilizing an 8-arm
416 radial maze and a step-down avoidance task – to assess spatial and short-term memory
417 in rats. Conducted approximate 82 days post-surgical and chemical castration, the study
418 concluded that castration deteriorates memory function [71]. In contrast, our findings,
419 based on BM test in castrated mice, suggest an enhancement in cognitive performance.
420 Several factors could account for these divergent outcomes. First, the timing of
421 cognitive assessments post-castration differed between the studies. Our behavioral tests
422 were performed on 12-13month old mice, nearly 10-11 months after castration or sham
423 operations. It is plausible that the benefits of castration on spatial memory may not be
424 readily apparent in younger rodents but become more pronounced with age. Second,
425 the choice of behavioral tasks could also contribute to the observed discrepancies. The

426 step-down inhibitory avoidance task, employed in the previous study, uses immediate
427 electric shocks as stimuli to evaluate aversive memory, while the 8-arm radial maze
428 task requires deprivation of food and/or water for animals. Electric shock is a type of
429 psychological stress for rodents [72]. Mounting evidence suggests that testosterone
430 significantly modulates physiological responses to stressors [73]; thus, the markedly
431 reduced testosterone levels in castrated mice could potentially confound the evaluation
432 of cognitive performance. To mitigate potential confounders, we opted for less stressful
433 tasks – namely BM, OF and NOR tests. Our results from the BM test indicate that
434 castration not only extends lifespan but also attenuates cognitive decline in older mice.
435 This suggests that the castration model offers a nuanced understanding of aging, one
436 that incorporates both longevity and cognitive preservation.

437 Sex as a key determinant biological variable has been historically overlooked
438 despite sexual dimorphism can be observed everywhere. On one hand, the bias toward
439 using male subjects in biomedical research has often been justified by the desire to
440 minimize variability, particularly traits influenced by the female estrous cycle [8]. This
441 male-centric focus has inadvertently limited our understanding of tissue function and
442 disease mechanisms from a sex-specific perspective, thereby highlighting the pressing
443 need for more inclusive animal models. On the other hand, straightforwardly comparing
444 male with female is generally applied in the increasingly emphatic but still limited sex-
445 difference studies, which made the leading mechanisms hard to recognize due to
446 complicated variables between male and female in both genetic and non-genetic aspects.
447 To broaden the feasibility and practicability of applying castration model in sex-
448 dependent biological queries, we tested the differences of tumor drugs-induced tissue
449 injuries among the three groups of mice. More sever renal damages were observed in
450 male than female after cisplatin treatment at both young and old ages [74]; however,
451 the roles of genetic and non-genetic co-determinants involved in this process are still
452 elusive. Rostami et al. found that 1 week post-castration rats with low dosage treatment
453 of TS rather than high dosage, were more tolerant with cisplatin nephrotoxicity [75],
454 while our pathological assays showed that castration deteriorated the renal toxicity.
455 Taken together, we believe that the balanced levels of TS are essential to defense the
456 toxicity. In summary, our study, in conjunction with methylation data in sheep [9],
457 advocates for the castration model as a promising approach. It effectively "feminizes"
458 males at multiple molecular levels through alterations in SHs, while preserving the
459 somatic male genotype. This unique duality positions the castration model as a useful

tool for distinguishing between hormone-induced sex differences and genotypic sex, broadening its utility beyond the scope of aging research.

Our comprehensive metabolomic and transcriptomic profiling across multiple tissues at both young and old life stages offers compelling insights. We observed multiple lipid related pathways were identified recurrently in comparisons of both "shamF *vs* shamM" and "casM *vs* shamM", and reduced lipid peroxidation in both casM and shamF, indicative of a shared molecular pathway that may contribute to healthier aging. Moreover, our data indicates that castration significantly attenuates the molecular differences mediated by sex and/or sex hormones across multiple omic layers. Driven by the need for a stable and broadly applicable model for the study of sex-dependent responses to cancer therapy, we further extended our exploration to include the feasibility of the castration model in assessing cancer drug toxicities, in addition to examining the healthy aging phenotype. These explorations and findings collectively underscore the castration model's versatility and its untapped potential for advancing our understanding of sex differences across various physiological and pathological landscapes.

476 **METHODS**

477 **Animals, surgical castration procedures, and sample collections**

478 C57/BL6 mice were purchased from Zhuhai BesTest Bio-Tech Co,.Ltd. and housed in
479 the animal facility of Shenzhen TopBiotech Co., Ltd (Shenzhen, China) under
480 pathogen-free condition with free access to chow and water. Male and female mice at
481 8 weeks old were anesthetized by isoflurane for castration (testicles removed) or sham
482 procedures. Mice were placed on a warm pad after suture, then transferred to cages
483 while awake. 4-weeks post-castration/sham operations, serum was collected for steroid
484 hormone detection and untargeted metabolites analysis while liver and kidney were
485 dissected for untargeted metabolites analysis and RNA-seq (n=3-6/group).
486 Castrated/sham mice at 12-13m old were subjected to behavioral tests and were
487 sacrificed for sample collection at 18m. At 18m, serum was used for untargeted
488 metabolomics while liver and kidneys were dissected for both untargeted metabolomics
489 and RNA-seq (n=3-6/group). The animal study protocol was approved by the Animal
490 Ethics Review Board of Shenzhen TopBiotech Animal Facilities (No. TOP-IACUC-
491 2021-0100).

492

493 **Sample treatment for targeted steroid hormone spectrum detection**

494 50 μL serum was thawed and vortexed for 30s following by mixture with purified H_2O,
495 internal standard working solution and methanol. The well mixed samples were then
496 subjected to repeated 13000 rpm centrifuge for 10 minutes (mins) under 4°C. The
497 supernatant was retained further purified with OASIS PRiME HLB uElution (SPE).
498 200 μL methanol and 200 μL H_2O were separately used to wash and equilibrate the SPE
499 cartridges. The supernatant was loaded to the equilibrated cartridges and then washed
500 by 200 μL 10% ACN/H_2O (v/v) and 200 μL Hexane. The flow-through fraction was
501 discarded. Rinse the cartridge was with 40 μL 90% ACN/H_2O (v/v) and collect the
502 cluent. Add 60 μL H_2O to the cluent and shake the mixture for 3 mins. The final mixture
503 and the same volume of isotopically-labelled internal standards were subjected to
504 UHPLC-MS/MS analysis.

505 **Serum sample preparation for untargeted MS analysis**

506 150 μL methanol which was premixed with isotopically-labelled internal standard
507 compounds was added to 50 μL mouse serum and vortexed for 30 seconds to mix well.
508 The mixture was then sonicated for 10 mins in ice water bath and incubated for 1 h at -

509 40 °C to precipitate proteins. After 15-min high-speed centrifugation, the supernatant
510 was used for MS analysis. An equal aliquot of the supernatants obtained from each
511 serum sample was mixed as the quality control (QC).
512
513 **Kidney/liver sample preparation for untargeted MS analysis**
514 10-25 mg tissues were submerged with extraction solution (methanol:water = 3: 1, with
515 isotopically-labelled internal standard mixture) and homogenized in ice-water bath.
516 Incubate homogenized samples for 1 h at -40°C and centrifuge at 12000 rpm for 15 min
517 at 4 °C. The supernatant was retained for MS analysis. A volume matched quality
518 control (QC) sample was prepared for MS.
519
520 **UHPLC-MS/MS analysis for targeted steroid hormone spectrum**
521 EXIONLC System (Sciex) equipped with a Waters Acquity Uplc Bch C8 column was
522 utilized for UHPLC analysis at Biotree Technology Co., Ltd. Assay development was
523 applied by SCIEX 6500+ triple quadrupole mass spectrometer (Sciex) with an IonDrive
524 Turbo V electrospray ionization (ESI) interface, under multiple reaction monitoring
525 (MRM) module. MassLynx Work Station Software (Version 4.1) was employed for
526 MRM data acquisition and preprocessing.
527
528 **UHPLC-MS/MS untargeted metabolomics analysis**
529 T3 chromatographic column with affinities to both lipid and hydrophile at Biotree
530 Technology Co., Ltd was used to acquire the metabolome of castrated male (casM),
531 sham male (shamM) and sham female (shamF) mice by Orbitrap mass spectrometer.
532 Joint negative (NEG) and positive (POS) ionization modes were employed for
533 detecting metabolites based on their mass to charge ratios. Raw data was converted to
534 the mzXML format using ProteoWizard platform (https://proteowizard.sourceforge.io/)
535 and processed with an in-house R script and XCMS tool [76] for peak detection,
536 extraction, alignment, and integration. Data was subjected to fragment extracted ion
537 chromatogram (MS^2) annotations as previously described [77], MS^2 metabolites with
538 scores > 0.3 were retained for next-step analysis. These compounds were mapped to
539 Human Metabolome Database (HMDB) and classified into multiple categories. The
540 biggest category under both NEG and POS modes is lipid and lipid-like molecules,
541 which counts for ≥ 30% identified metabolites (**Figure 3a-b, Supplementary Table 2-**
542 **3**). Compounds from NEG and POS modes were merged for down-stream analysis.

543

544 **Behavioral tests**

545 Three groups of mice include casM, shamM and shamF at 12-13 months old (n= 6-13)
546 were subjected to BM, OF and NOR tasks. A 60 cm high, 120 cm-diameter and 60 mm
547 thick circular wheeled PVC slab with 25 cm-diameter holes was used for BM tests. A
548 modified protocol was employed following the standard methods in previous study [78].
549 Briefly, mice were firstly trained in continuous 7 days to find the escape hole within 4
550 mins; if failed, mice were finally guided to the target hole gently. Mice were subjected
551 to the probe trial on day 8. OF test was applied to test the exploratory behavior and
552 general activity of mice, mice were placed in an enclosure, rectangular tank with
553 surrounding walls for 5 mins, distance moved, time spent moving, rearing, and change
554 in activity over time for each mouse were recorded. NOR test was performed following
555 previous study [79]. Mice were placed in the empty tank for 10 mins on day1; day 2,
556 two objects were placed in the tank, and mice were allowed for 10 mins to explore; one
557 of the objects was replaced by a new one on day 3, and time spent for exploration (TE)
558 within 5 mins for each object was recorded. NOR index was calculated via this
559 formulation: NOR index = new object TE- old object TE/ Total TE. Mice behaviors
560 during these tests were recorded and analyzed by ANY-MAZE software
561 (https://www.any-maze.com/).

562

563 **Western-blot**

564 Total protein was isolated on ice by cell & tissue lysis buffer (Cat#P0013, Beyontime,
565 China) and quantitated using BCA assay kit (Cat#P0012, Beyontime, China).
566 Approximate 15ug protein was used for western-blot assays following previous
567 protocols [65]. Antibodies for MDA, SOD1 and SOD2were purchased from abcam
568 (Cat# ab243066, ab13498 and ab13533), GAPDH was purchased from Beyontime
569 (Cat# AF0006).

570

571 **RNA extraction for RNA-seq analysis**

572 Total RNA was extracted using Trizol reagents (Invitrogen Cat#15596026) as we have
573 described before [80]. PolyA-tailed RNA was enriched for constructing 150bp pair-end
574 RNA-sequencing libraries using MGISEQ-2000RS kit (MGI Cat#1000012555), and
575 sequenced by DNBseq MGI2000 platform at BGI genomics Co,. Ltd.

576

577 **Cisplatin administration**

578 Mice were administrated for intraperitoneal injection of cisplatin (Cat# 232120, sigma)
579 at 4 weeks post-castration/sham operations, with a dosage of 5 mg/kg every72 hours
580 for 2 times. Mice were sacrificed 48 hours after cisplatin treatment for the collection of
581 liver and kidney tissues.

582

583 **Histopathological analysis**

584 For liver and kidney tissue examination, samples were first fixed in 10% formalin
585 solution for 48 hours, followed by paraffin embedding. Sections of 3 μm thickness were
586 then prepared for histological analysis. Hematoxylin and Eosin (H & E) and Periodic
587 Acid-Schiff (PAS) staining were performed according to established protocols. Liver
588 injury was evaluated by visually inspecting the patterns of steatosis, sinusoidal
589 congestion, and hemorrhage. Renal injury was quantitatively assessed using the scoring
590 criteria established in a previous study [81].

591

592 **Identification of significant altered metabolites (SAMs) and differentially**
593 **expressed genes (DEGs)**

594 A strict pipeline was applied to identify SAMs. Firstly, the normalized peak values of
595 metabolites were subjected to unsupervised principal component analysis (PCA) and
596 then administrated to supervised orthogonal projections to latent structures-
597 discriminate analysis (OPLS-DA) for data modeling by commercial SIMCA software
598 (V16.0.2). A 7-fold cross validation was employed for model selection. To evaluate the
599 predictive power and robustness of OPLS-DA model, a 200-times-permutations was
600 performed and the value of variable importance in the projection (VIP) of the first
601 principal component in OPLS-DA analysis was calculated which represents the
602 contribution of each variable to the model. Metabolites with VIP > 1 and students' t-
603 test p-value < 0.05 were recognized as SAMs. For DEG identification, quality control
604 was performed for raw RNA-seq reads by SolexaQA (-h 30, -l 30) [82]. Cleaned reads
605 were subjected to Hisat2 [83] for mapping. Cufflinks package [84] was utilized to
606 calculate the Fragments Per Kilobase of transcript per Million mapped reads (FPKM)
607 values and to identify DEGs use FDR < 0.05 as the cutoff value.

608

609 **Expression trend clustering analysis**

610 To identify expression trend patterns of metabolites among the serum samples of 12w

casM, shamM and shamF, the union of SAMs across three pairwise comparisons in Figure 4A were analyzed by Mfuzz package (c=9, m =1.25) (Figure 4E) [85]. To illustrate genes that potentially related with taurine, the expression levels (FPKM values) of all the annotated genes in kidneys and livers at 12w and 18m casM, shamM and shamF mice, were also subjected to Mfuzz package [85] for clustering (c=9, m =1.25). The semi-quantitative concentrations of taurine were plotted as stack lines. Genes that show similar expression trend with taurine in all the tissues were retained (Figure 5F-G).

Hierarchical clustering analysis

Hierarchical clustering analysis for SH levels after castration/sham treatments (Figure 2A), the expression of 51 taurine related genes (Figure 5E), serum metabolomic profiles among casM, shamM and shamF using (Figure 4B) and tissue RNA-seq gene expression profiles (Figure 6C), were performed by Hclust function in R platform using Euclidean distance metric and complete lineage. The z-score standardized SH levels and expression levels of taurine related genes after clustering were visualized via heatmap using pheatmap 1.0.12 package.

Enrichment analysis of SAMs

SAMs were subjected for topology-based KEGG pathway enrichment analysis using MetaboAnalyst with default parameters [86]. Differential abundance (DA) scores [87] were calculated for the significant enrichment terms using this formula: DA scores =

$$\frac{\text{Up regulated metabolite No.in the pathway} - \text{Downregulated metabolite No. in the pathway}}{\text{Total metabolite No.of the pathway}}$$

Joint metabolome & transcriptome analysis

To examine the interplay between metabolomics and other transcriptomics layers, SAMs and DEGs were used for joint metabolome & transcriptome enrichment analysis against KEGG pathways via MetaboAnalystR under joint-analysis module by hypergeometric test with default parameters. FDR <.0.05 was applied as the cut-off value [86, 88].

REFERENCE

1. Lemaître, J.-F., et al., *Sex differences in adult lifespan and aging rates of mortality across wild mammals.* Proceedings of the National Academy of Sciences, 2020. **117**(15): p. 8546-8553.
2. Martínez-Sellés, M., et al., *Sex-Related Differences in Centenarians and Their Hearts.* J Am Geriatr Soc, 2016. **64**(2): p. 444-6.
3. Evert, J., et al., *Morbidity profiles of centenarians: survivors, delayers, and escapers.* J Gerontol A Biol Sci Med Sci, 2003. **58**(3): p. 232-7.
4. Miszko, T.A., et al., *Effect of strength and power training on physical function in community-dwelling older adults.* J Gerontol A Biol Sci Med Sci, 2003. **58**(2): p. 171-5.
5. Marais, G.A.B., et al., *Sex gap in aging and longevity: can sex chromosomes play a role?* Biol Sex Differ, 2018. **9**(1): p. 33.
6. Horstman, A.M., et al., *The role of androgens and estrogens on healthy aging and longevity.* J Gerontol A Biol Sci Med Sci, 2012. **67**(11): p. 1140-52.
7. Iorga, A., et al., *The protective role of estrogen and estrogen receptors in cardiovascular disease and the controversial use of estrogen therapy.* Biol Sex Differ, 2017. **8**(1): p. 33.
8. Mauvais-Jarvis, F., A.P. Arnold, and K. Reue, *A Guide for the Design of Pre-clinical Studies on Sex Differences in Metabolism.* Cell Metab, 2017. **25**(6): p. 1216-1230.
9. Sugrue, V.J., et al., *Castration delays epigenetic aging and feminizes DNA methylation at androgen-regulated loci.* Elife, 2021. **10**.
10. Jiang, N., et al., *Prepubertal castration eliminates sex differences in lifespan and growth trajectories in genetically heterogeneous mice.* Aging Cell, 2023. **22**(8): p. e13891.
11. Min, K.J., C.K. Lee, and H.N. Park, *The lifespan of Korean eunuchs.* Curr Biol, 2012. **22**(18): p. R792-3.
12. Zhang, Z., et al., *Wnt/β-catenin signaling promotes aging-associated hair graying in mice.* Oncotarget, 2017. **8**(41): p. 69316-69327.
13. Bresilla, D., et al., *The sex-specific metabolic signature of C57BL/6NRj mice during aging.* Sci Rep, 2022. **12**(1): p. 21050.
14. Raldiris, T.L., et al., *Cognitive control beliefs and cognitive functioning in mid-to late-life.* Br J Dev Psychol, 2021. **39**(2): p. 269-281.
15. Kraemer, W.J., et al., *Growth Hormone(s), Testosterone, Insulin-Like Growth Factors, and Cortisol: Roles and Integration for Cellular Development and Growth With Exercise.* Front Endocrinol (Lausanne), 2020. **11**: p. 33.
16. van den Beld, A.W., et al., *The physiology of endocrine systems with ageing.* Lancet Diabetes Endocrinol, 2018. **6**(8): p. 647-658.
17. Crafa, A., et al., *The Burden of Hormonal Disorders: A Worldwide Overview With a Particular Look in Italy.* Front Endocrinol (Lausanne), 2021. **12**: p. 694325.
18. Turcu, A., et al., *Adrenal androgens and androgen precursors-definition, synthesis, regulation and physiologic actions.* Compr Physiol, 2014. **4**(4): p. 1369-81.
19. Lin, C., et al., *Effects on longevity extension and mechanism of action of carnosic acid in Caenorhabditis elegans.* Food Funct, 2019. **10**(3): p. 1398-1410.
20. Das, U.N., *Ageing: Is there a role for arachidonic acid and other bioactive lipids? A review.* J Adv Res, 2018. **11**: p. 67-79.

21. Wortmann, S.B. and J.A. Mayr, *Choline-related-inherited metabolic diseases-A mini review.* J Inherit Metab Dis, 2019. **42**(2): p. 237-242.
22. Igarashi, M., et al., *Chronic nicotinamide mononucleotide supplementation elevates blood nicotinamide adenine dinucleotide levels and alters muscle function in healthy older men.* npj Aging, 2022. **8**(1): p. 5.
23. Hong, Y., et al., *Association between plasma Vitamin B5 levels and all-cause mortality: A nested case-control study.* J Clin Hypertens (Greenwich), 2022. **24**(7): p. 945-954.
24. Mohammadi, E., et al., *Protective effect of crocin against d-galactose-induced aging in mice.* Avicenna J Phytomed, 2018. **8**(1): p. 14-23.
25. Lu, H.J., et al., *Ruscogenin ameliorates diabetic nephropathy by its anti-inflammatory and anti-fibrotic effects in streptozotocin-induced diabetic rat.* BMC Complement Altern Med, 2014. **14**: p. 110.
26. Sova, M. and L. Saso, *Natural Sources, Pharmacokinetics, Biological Activities and Health Benefits of Hydroxycinnamic Acids and Their Metabolites.* Nutrients, 2020. **12**(8).
27. Heo, H.J., et al., *Effects of oleamide on choline acetyltransferase and cognitive activities.* Biosci Biotechnol Biochem, 2003. **67**(6): p. 1284-91.
28. Ano, Y., et al., *Preventive effects of a fermented dairy product against Alzheimer's disease and identification of a novel oleamide with enhanced microglial phagocytosis and anti-inflammatory activity.* PLoS One, 2015. **10**(3): p. e0118512.
29. Wang, C., et al., *Hydroxyeicosapentaenoic acids and epoxyeicosatetraenoic acids attenuate early occurrence of nonalcoholic fatty liver disease.* Br J Pharmacol, 2017. **174**(14): p. 2358-2372.
30. Nagatake, T., et al., *12-Hydroxyeicosapentaenoic acid inhibits foam cell formation and ameliorates high-fat diet-induced pathology of atherosclerosis in mice.* Sci Rep, 2021. **11**(1): p. 10426.
31. Rokicki, J., et al., *Daily Carnosine and Anserine Supplementation Alters Verbal Episodic Memory and Resting State Network Connectivity in Healthy Elderly Adults.* Front Aging Neurosci, 2015. **7**: p. 219.
32. Cai, H., et al., *Metabolomic signatures for liver tissue and cecum contents in high-fat diet-induced obese mice based on UHPLC-Q-TOF/MS.* Nutr Metab (Lond), 2021. **18**(1): p. 69.
33. Anderson, A., et al., *7-Ketocholesterol in disease and aging.* Redox Biol, 2020. **29**: p. 101380.
34. Kanter, R. and B. Caballero, *Global gender disparities in obesity: a review.* Advances in nutrition, 2012. **3**(4): p. 491-498.
35. Bilstein, A., et al., *Ectoine in the Treatment of Irritations and Inflammations of the Eye Surface.* Biomed Res Int, 2021. **2021**: p. 8885032.
36. Zhao, M., et al., *Resolvin D2 and its receptor GPR18 in cardiovascular and metabolic diseases: A promising biomarker and therapeutic target.* Pharmacol Res, 2023. **195**: p. 106832.
37. Singh, P., et al., *Taurine deficiency as a driver of aging.* Science, 2023. **380**(6649): p. eabn9257.
38. Warden, C., J.M. Barnett, and M.A. Brantley, Jr., *Taurocholic acid inhibits features of age-related macular degeneration in vitro.* Exp Eye Res, 2020. **193**: p. 107974.
39. Wolf, P.G., et al., *Effects of taurocholic acid metabolism by gut bacteria: A controlled feeding trial in adult African American subjects at elevated risk for*

colorectal cancer. Contemp Clin Trials Commun, 2020. **19**: p. 100611.
40. Ur Rahman, S., A. Qadeer, and Z. Wu, *Role and Potential Mechanisms of Nicotinamide Mononucleotide in Aging.* Aging Dis, 2023.
41. Harrison, F.E., *A critical review of vitamin C for the prevention of age-related cognitive decline and Alzheimer's disease.* J Alzheimers Dis, 2012. **29**(4): p. 711-26.
42. Pelton, R.B. and R.J. Williams, *Effect of pantothenic acid on the longevity of mice.* Proc Soc Exp Biol Med, 1958. **99**(3): p. 632-3.
43. Ishiguro, K., *Aging effect of blood pantothenic acid content in female.* Tohoku J Exp Med, 1972. **107**(4): p. 367-72.
44. Dave, N., et al., *Dietary choline intake is necessary to prevent systems-wide organ pathology and reduce Alzheimer's disease hallmarks.* Aging Cell, 2023. **22**(2): p. e13775.
45. Wang, J., et al., *Emerging Roles of Ganoderma Lucidum in Anti-Aging.* Aging Dis, 2017. **8**(6): p. 691-707.
46. Kim, Y.J., et al., *Oleanolic Acid Protects the Skin from Particulate Matter-Induced Aging.* Biomol Ther (Seoul), 2021. **29**(2): p. 220-226.
47. Ványolós, A., et al., *Extracts and Steroids from the Edible Mushroom Hypholoma lateritium Exhibit Anti-Inflammatory Properties by Inhibition of COX-2 and Activation of Nrf2.* Chem Biodivers, 2020. **17**(9): p. e2000391.
48. Li, Z., et al., *Graveoline Analogs Exhibiting Selective Acetylcholinesterase Inhibitory Activity as Potential Lead Compounds for the Treatment of Alzheimer's Disease.* Molecules, 2016. **21**(2): p. 132.
49. Murakami, S., et al., *Taurine ameliorates cholesterol metabolism by stimulating bile acid production in high-cholesterol-fed rats.* Clin Exp Pharmacol Physiol, 2016. **43**(3): p. 372-8.
50. Jakaria, M., et al., *Taurine and its analogs in neurological disorders: Focus on therapeutic potential and molecular mechanisms.* Redox Biol, 2019. **24**: p. 101223.
51. Guy, J. and M.G. Peters, *Liver disease in women: the influence of gender on epidemiology, natural history, and patient outcomes.* Gastroenterol Hepatol (N Y), 2013. **9**(10): p. 633-9.
52. Guo, Q., et al., *Taurine Attenuates Oxidized Fish Oil-Induced Oxidative Stress and Lipid Metabolism Disorder in Mice.* Antioxidants (Basel), 2022. **11**(7).
53. Qi, W., et al., *The ω-3 fatty acid α-linolenic acid extends Caenorhabditis elegans lifespan via NHR-49/PPARα and oxidation to oxylipins.* Aging Cell, 2017. **16**(5): p. 1125-1135.
54. Hajri, T., A. Pronczuk, and K. Hayes, *Linoleic acid-rich diet increases hepatic taurine and cholesterol 7α-hydroxylase activity in conjunction with altered bile acid composition and conjugation in gerbils.* The Journal of nutritional biochemistry, 1998. **9**(5): p. 249-257.
55. Wang, H., et al., *Mutations in SREBF1, Encoding Sterol Regulatory Element Binding Transcription Factor 1, Cause Autosomal-Dominant IFAP Syndrome.* Am J Hum Genet, 2020. **107**(1): p. 34-45.
56. Birder, L.A. and E.K. Jackson, *Dysregulated Purine Metabolism Contributes to Age-Associated Lower Urinary Tract Dysfunctions.* Adv Geriatr Med Res, 2021. **3**(4).
57. Sekiya, M., et al., *SREBP-1-independent regulation of lipogenic gene expression in adipocytes.* J Lipid Res, 2007. **48**(7): p. 1581-91.
58. Liu, Y., et al., *The Role of PPAR-δ in Metabolism, Inflammation, and Cancer:*

Many Characters of a Critical Transcription Factor. Int J Mol Sci, 2018. **19**(11).
59. Chatterjee, I., et al., *Vitamin D receptor promotes healthy microbial metabolites and microbiome.* Sci Rep, 2020. **10**(1): p. 7340.
60. Penn, D.J., S.M. Zala, and K.C. Luzynski, *Regulation of Sexually Dimorphic Expression of Major Urinary Proteins.* Front Physiol, 2022. **13**: p. 822073.
61. Lu, Y., Z. Pang, and J. Xia, *Comprehensive investigation of pathway enrichment methods for functional interpretation of LC-MS global metabolomics data.* Brief Bioinform, 2023. **24**(1).
62. Johnstone, T.C., G.Y. Park, and S.J. Lippard, *Understanding and improving platinum anticancer drugs--phenanthriplatin.* Anticancer Res, 2014. **34**(1): p. 471-6.
63. Marcu, L.G., *Gender and Sex-Related Differences in Normal Tissue Effects Induced by Platinum Compounds.* Pharmaceuticals (Basel), 2022. **15**(2).
64. Nematbakhsh, M., et al., *Gender difference in Cisplatin-induced nephrotoxicity in a rat model: greater intensity of damage in male than female.* Nephrourol Mon, 2013. **5**(3): p. 818-21.
65. Jiang, J., et al., *Decoding the role of long noncoding RNAs in the healthy aging of centenarians.* Brief Bioinform, 2021. **22**(5).
66. Kent, M.S., et al., *Longevity and mortality in cats: A single institution necropsy study of 3108 cases (1989-2019).* PLoS One, 2022. **17**(12): p. e0278199.
67. Svedlund Eriksson, E., et al., *Castration of Male Mice Induces Metabolic Remodeling of the Heart.* J Endocr Soc, 2022. **6**(11): p. bvac132.
68. Zhang, X., et al., *Castration of male mice prevents the progression of established angiotensin II-induced abdominal aortic aneurysms.* J Vasc Surg, 2015. **61**(3): p. 767-76.
69. Ghosh, T.S., F. Shanahan, and P.W. O'Toole, *The gut microbiome as a modulator of healthy ageing.* Nat Rev Gastroenterol Hepatol, 2022. **19**(9): p. 565-584.
70. McGee, J.S. and C. Huttenhower, *Of mice and men and women: Sexual dimorphism of the gut microbiome.* Int J Womens Dermatol, 2021. **7**(5Part A): p. 533-538.
71. Shin, M.S., et al., *Long-term Surgical and Chemical Castration Deteriorates Memory Function Through Downregulation of PKA/CREB/BDNF and c-Raf/MEK/ERK Pathways in Hippocampus.* Int Neurourol J, 2019. **23**(2): p. 116-124.
72. Kim, J.Y., et al., *Mice subjected to uncontrollable electric shocks show depression-like behaviors irrespective of their state of helplessness.* Behav Brain Res, 2017. **322**(Pt A): p. 138-144.
73. Kutlikova, H.H., et al., *The effects of testosterone on the physiological response to social and somatic stressors.* Psychoneuroendocrinology, 2020. **117**: p. 104693.
74. Eshraghi-Jazi, F. and M. Nematbakhsh, *Sex Difference in Cisplatin-Induced Nephrotoxicity: Laboratory and Clinical Findings.* J Toxicol, 2022. **2022**: p. 3507721.
75. Rostami, B., et al., *Effect of testosterone on Cisplatin-induced nephrotoxicity in surgically castrated rats.* Nephrourol Mon, 2014. **6**(5): p. e21546.
76. Xia, J. and D.S. Wishart, *MSEA: a web-based tool to identify biologically meaningful patterns in quantitative metabolomic data.* Nucleic Acids Res, 2010. **38**(Web Server issue): p. W71-7.
77. Alseekh, S., et al., *Mass spectrometry-based metabolomics: a guide for annotation, quantification and best reporting practices.* Nat Methods, 2021.

18(7): p. 747-756.
78. Ederer, M.L., et al., *Voluntary Wheel Running in Old C57BL/6 Mice Reduces Age-Related Inflammation in the Colon but Not in the Brain.* Cells, 2022. **11**(3).
79. Lueptow, L.M., *Novel Object Recognition Test for the Investigation of Learning and Memory in Mice.* J Vis Exp, 2017(126).
80. Luo, Y.M., et al., *Insights into the mechanisms of triptolide nephrotoxicity through network pharmacology-based analysis and RNA-seq.* Front Plant Sci, 2023. **14**: p. 1144583.
81. Rong, S., et al., *The TIM-1:TIM-4 pathway enhances renal ischemia-reperfusion injury.* J Am Soc Nephrol, 2011. **22**(3): p. 484-95.
82. Cox, M.P., D.A. Peterson, and P.J. Biggs, *SolexaQA: At-a-glance quality assessment of Illumina second-generation sequencing data.* BMC Bioinformatics, 2010. **11**: p. 485.
83. Kim, D., B. Langmead, and S.L. Salzberg, *HISAT: a fast spliced aligner with low memory requirements.* Nat Methods, 2015. **12**(4): p. 357-60.
84. Trapnell, C., et al., *Differential gene and transcript expression analysis of RNA-seq experiments with TopHat and Cufflinks.* Nat Protoc, 2012. **7**(3): p. 562-78.
85. Kumar, L. and E.F. M, *Mfuzz: a software package for soft clustering of microarray data.* Bioinformation, 2007. **2**(1): p. 5-7.
86. Lu, Y., Z. Pang, and J. Xia, *Comprehensive investigation of pathway enrichment methods for functional interpretation of LC–MS global metabolomics data.* Briefings in Bioinformatics, 2022. **24**(1).
87. Su, G.-H., et al., *Radiogenomic-based multiomic analysis reveals imaging intratumor heterogeneity phenotypes and therapeutic targets.* Science Advances, 2023. **9**(40): p. eadf0837.
88. Lu, Y., Z. Pang, and J. Xia, *Comprehensive investigation of pathway enrichment methods for functional interpretation of LC–MS global metabolomics data.* Briefings in Bioinformatics, 2023. **24**(1): p. bbac553.

Author Contributions

J.J. conceived and designed this study; J.J. and W.W. wrote and revised this manuscript; S.Y. and F.L. provided necessary resources to this study; J.J. performed the metabolomics, RNA-seq analysis, and the western blot assay; N.G. and X.G performed the metabolomics analysis; Y.W. and G.W. performed the animal behavior tests; J. Q., and K. G. performed the sham/castration procedure; J.J., Y.W., G.W., J. Q., K. G., X.G and Y.L. did the mouse colony and tissue samples collection.

Acknowledgement

We acknowledge Ms. Jiahui Liu for her generous help for sample collection and Dr. Xinhui Liu for his kind help for assessing renal injury scores. This work was supported by Shenzhen Science and Technology Program (Grant No.RCBS20210706092341003) to J.J.

Declaration of interests

The authors declare that none of them has competing interests.

FIGURES

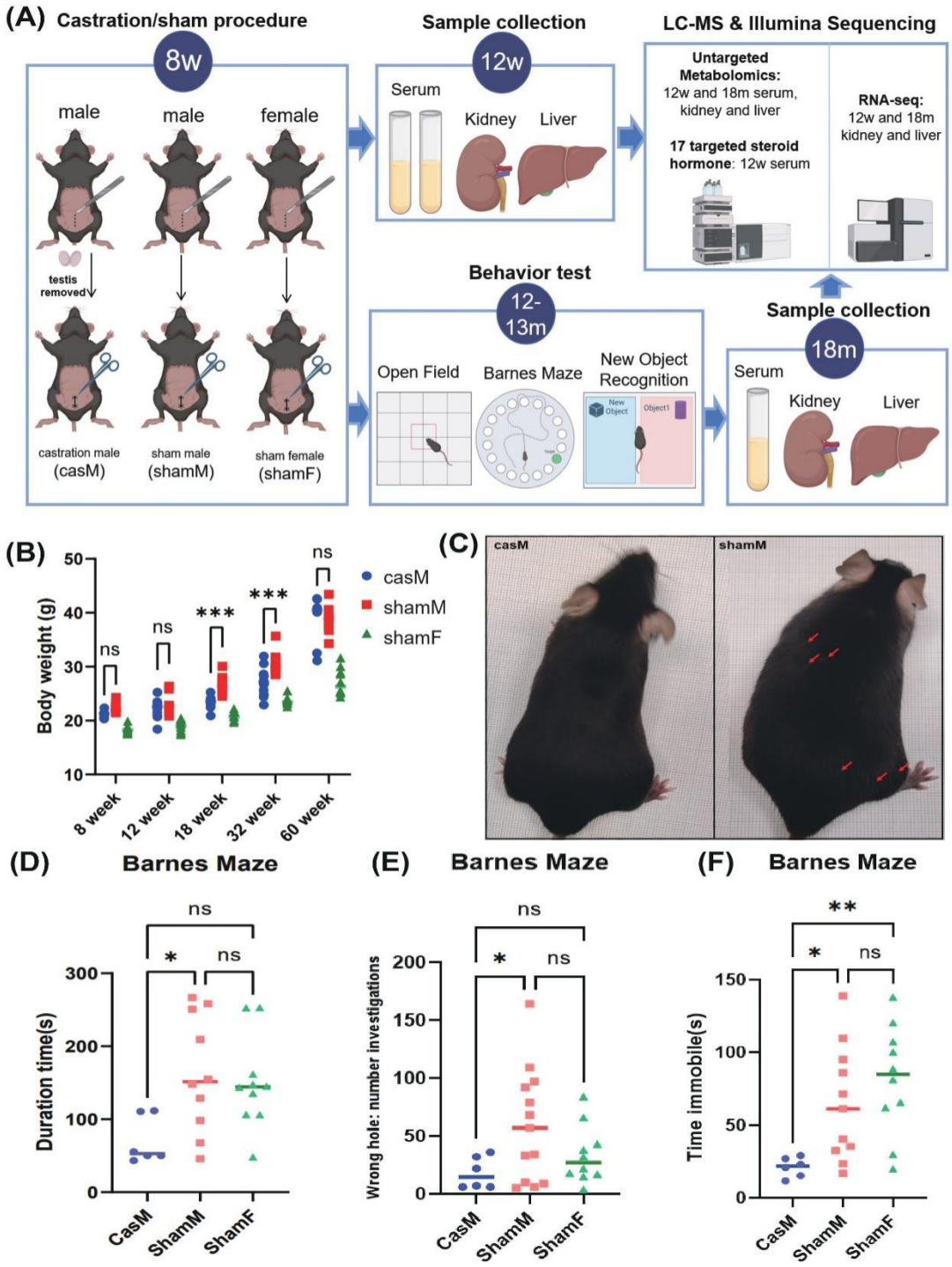

Figure 1. Overall study design as well as phenotypic and behavior tests of castration-mediated longevity. (**A**) Graphic illustration of the overall experimental design. (**B**) Body weight of casM, shamM and shamF mice from 8 to 60 weeks (n = 13, 12, 13 for casM, shamM, and shamF, respectively; unpaired students' t-test,***p < 0.001, ns: not significant) (**C**) More gray hairs (see red arrows) were observed in shamM than casM at 12-13 months old; (**D-F**) Analysis of BM tests results: duration time that mice have spent to find the correct target escape hole (**D**), exploration of

898 wrong holes numbers (**E**), and immobile time during the test (**F**) among casM (n=6),
899 shamM (n= 13) and shamF (n = 10) by One-Way ANOVA, * $p < 0.05$, $^{**}p < 0.01$, ns:
900 not significant.
901

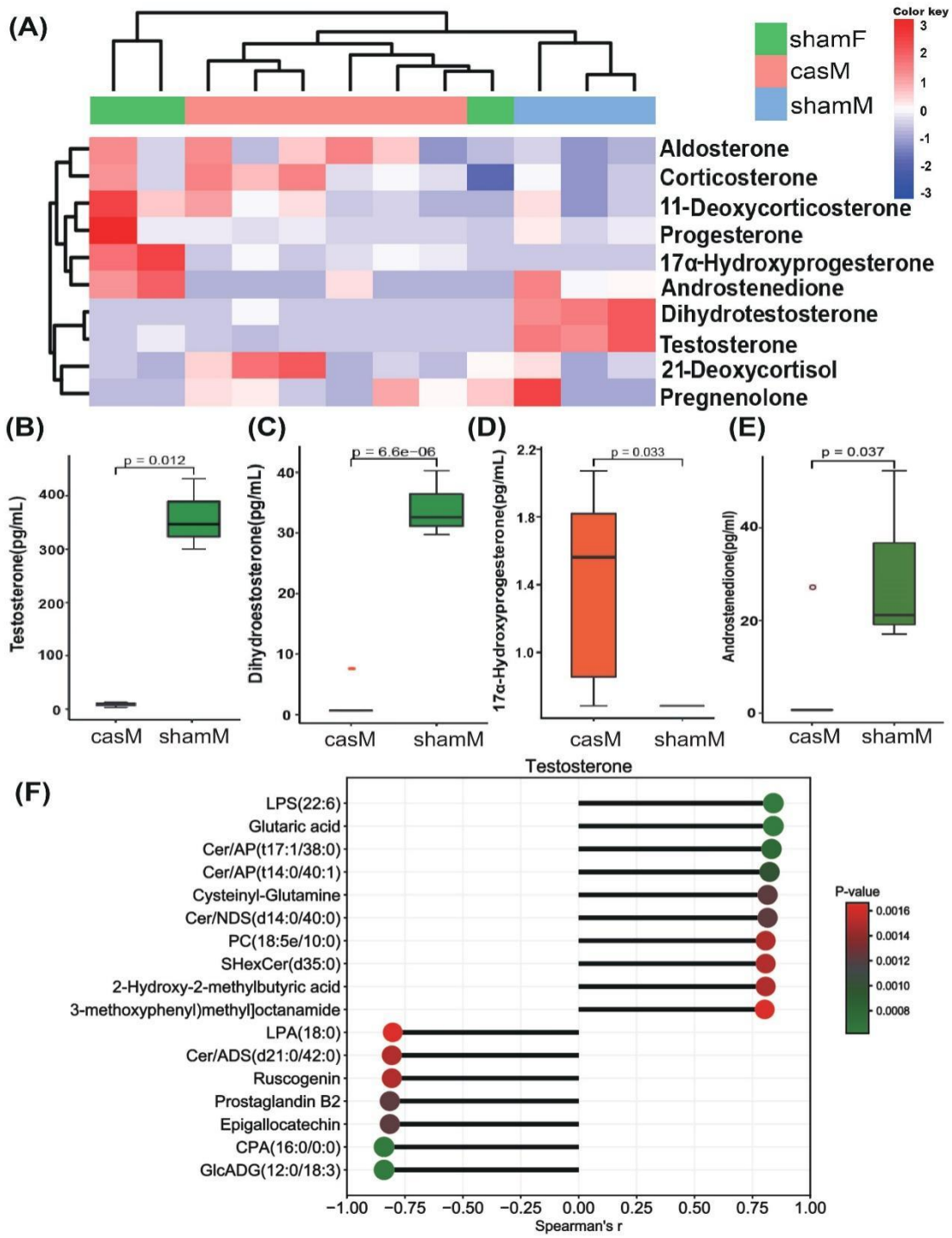

Figure 2. Alterations of the steroid hormones secretion induced by castration. (**A**) Hierarchical cluster heatmap of z-score standardized expression levels of 10 detectable steroid hormones among shamM, casM and shamF; (**B-E**) Comparisons of the quantitative levels of testosterone (**B**), dihydroestosterone (**C**), 17-hydroxyprogesterone (**D**) and androstenedione (**E**) between shamM and casM (unpaired students' t-test, *p*-values were shown on top); (**F**) List of compounds highly correlated with TS (Spearman's $|r| \geq 0.8$, $p \leq 0.001$).

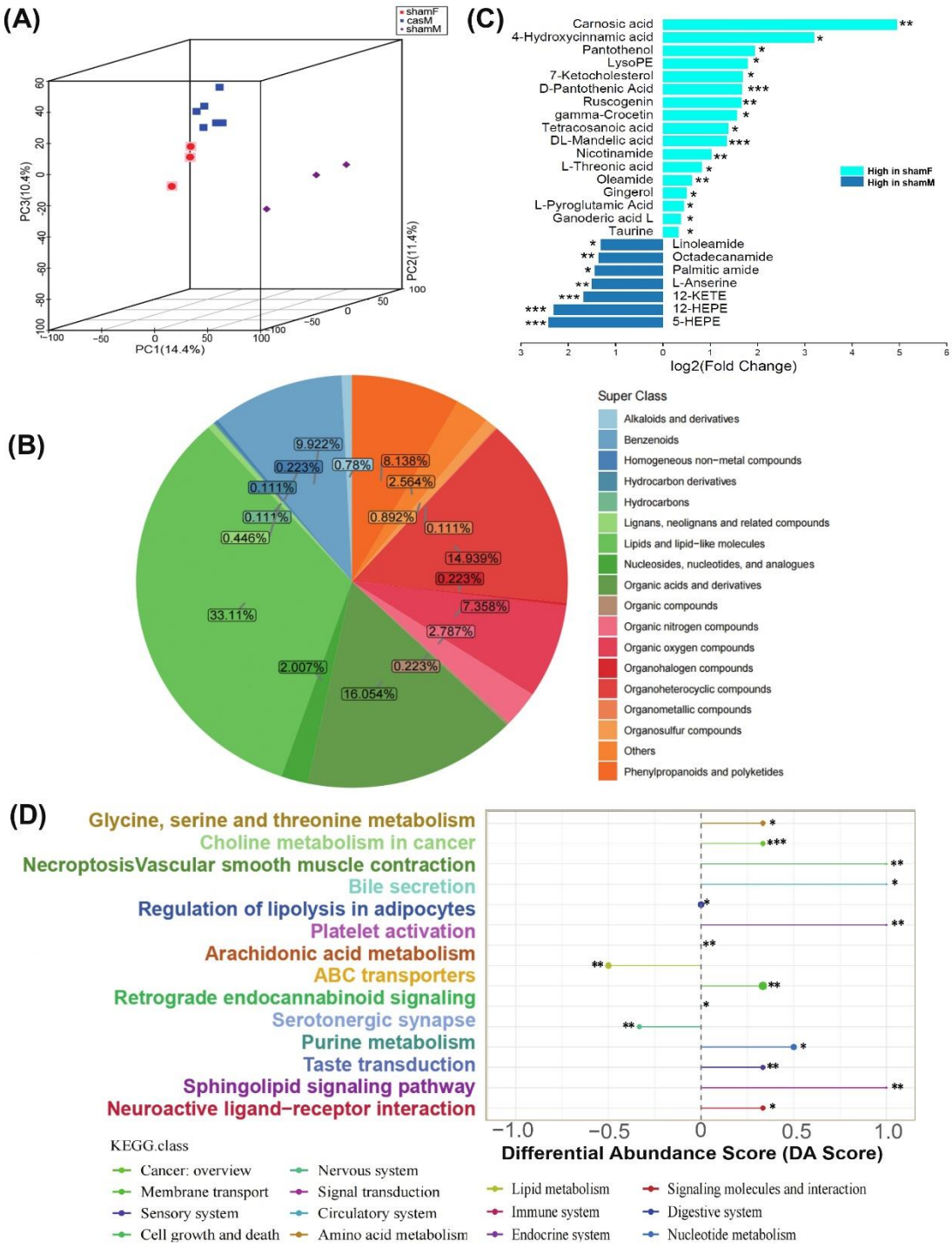

Figure 3. Characterizations of the 12w serum metabolomics. (**A**) PCA clustering of the serum untargeted metabolomics among casM, shamM and shamF; (**B**) Categories of the 1495 12w serum metabolites with high quality MS^2 annotations; (**C**) Representative SAMs between shamM and shamF that related with aging and healthy aging (unpaired students' t-test, $*p < 0.05$, $**p < 0.01$, $***p < 0.001$); (**D**) Differential abundance (DA) scores were calculated for the significant enrichment terms between shamM and shamF ($*p < 0.05$, $**p < 0.01$, $***p < 0.001$).

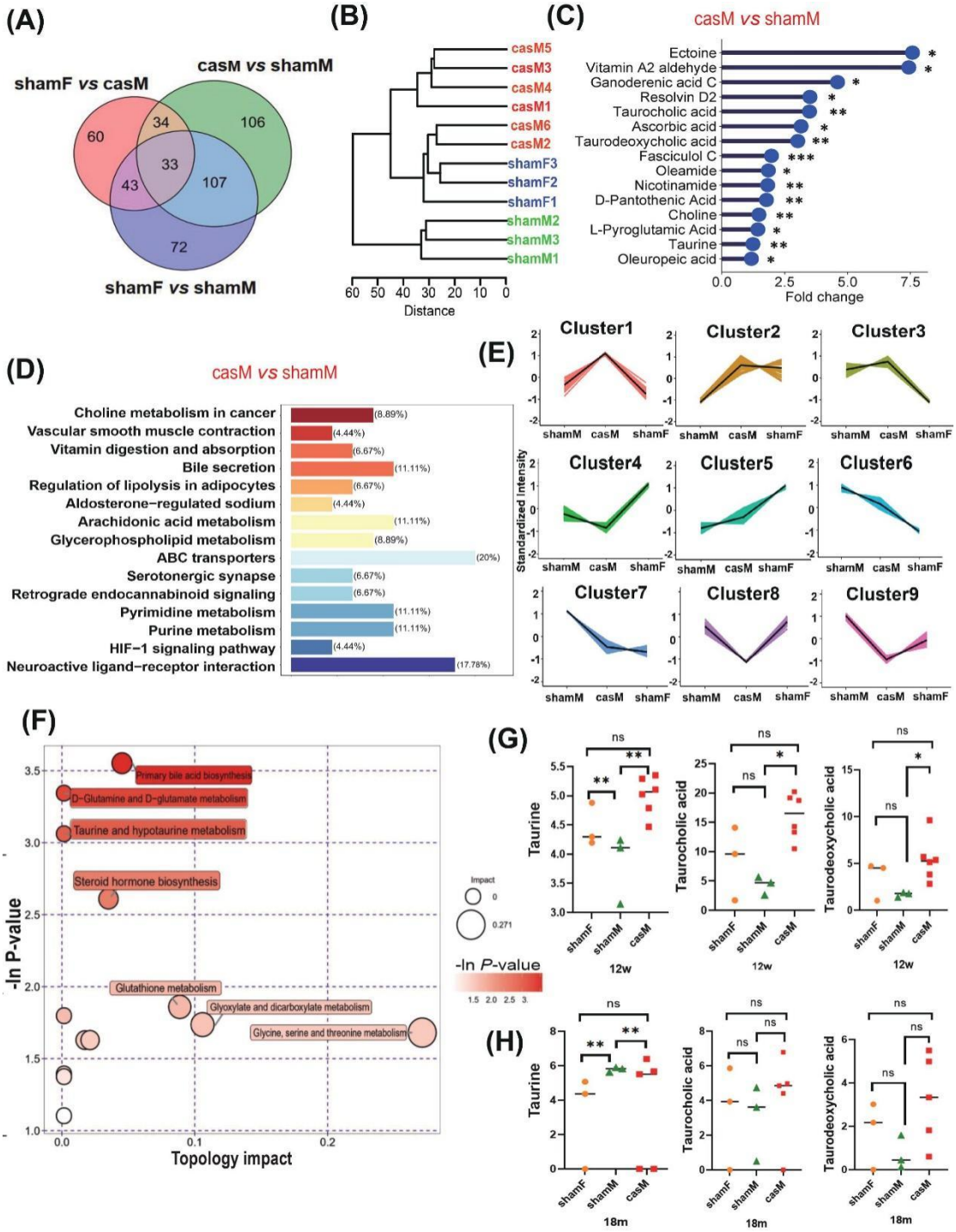

Figure 4. Identification of castration-specific metabolomic features in 12w mice. (**A**) Venny diagram of the serum SAMs identified from "shamF *vs* ShamM", "shamF *vs* casM" and "casM *vs* ShamM"; (**B**) Hierarchical clustering tree of different mouse groups using levels of compounds as input; (**C**) Representative food derived SAMs between casM and shamM (unpaired students' t-test, $*p < 0.05$, $**p < 0.01$, $***p < 0.001$); (D) Barplot of the KEGG enrichment terms using SAMs of "casM *vs* ShamM", percentage of hit compounds to total SAMs was calculated for each term; (**E**)

Expression patterns of merged SAMs among casM, shamM and shamF analyzed using mfuzzing clustering. Clusters 1 and 8 distinctively represent metabolites that are, respectively, highly and lowly detected specifically in casM. (**F**) Significantly enriched KEGG terms of metabolites highly expressed metabolites in casM (cluster 1 in **E**) calculated by topology-based pathway enrichment with topology impact shown in x-axis; (**G-H**) Comparisons of taurine, taurocholic acid and taurodeoxycholic acid among 12w (**G**) and 18m (**H**) shamF, sham and casM (One-Way ANOVA, $*p < 0.05$, $**p < 0.01$, ns: not significant).

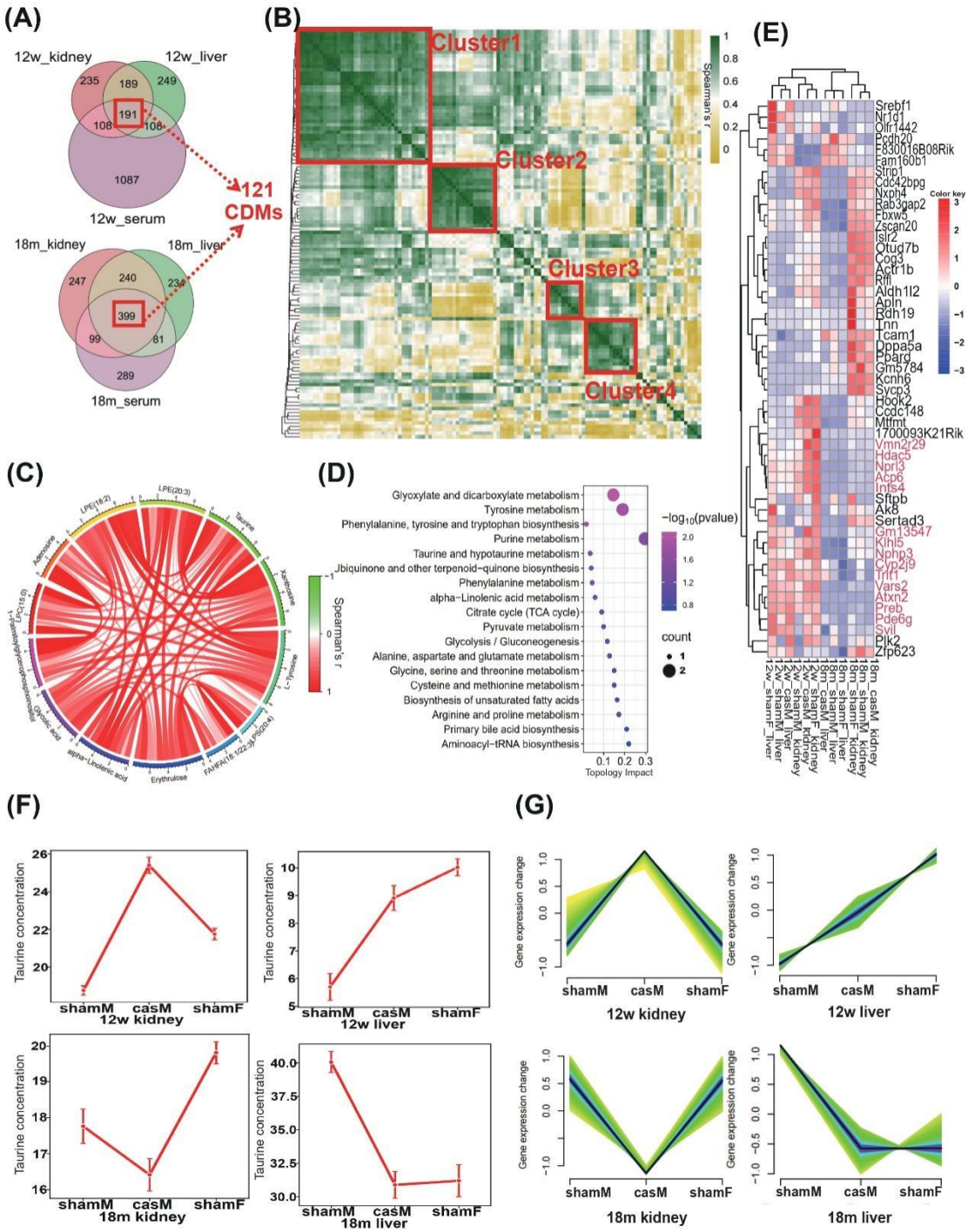

Figure 5. Co-expression analysis across serum, livers and kidneys identifies potential taurine-related regulators. (**A**) Venn diagram of detected compounds among serum, livers and kidneys across all the mouse groups at 12w and 18m, 121 commonly detected compounds (CDBs) were identified; (**B**) Co-expression analysis of the 121 CDBs revealed four major consensus clusters; (**C**) Correlation circos plot of the cluster 4 compounds in **B**; (**D**) Topology-based pathway enrichment analysis of the cluster 4 compounds in **B**, x-axis is the topology enrichment impact of hinted

943 compounds; (**E**) Hierarchical cluster heatmap of z-score standardized expression levels
944 of 51 taurine related genes in 12w and 18m kidneys and livers among shamM, shamF
945 and casM mice. Genes selectively reduced in 18m tissues are highlighted in red; (**F**)
946 Trends of taurine levels among shamM, shamF and casM across liver and kidney tissues
947 in 12w and 18m mice; (**F**) Mfuzzing clustering of the 51 taurine co-expressed genes
948 across liver and kidney tissues in 12w and 18m mice.
949

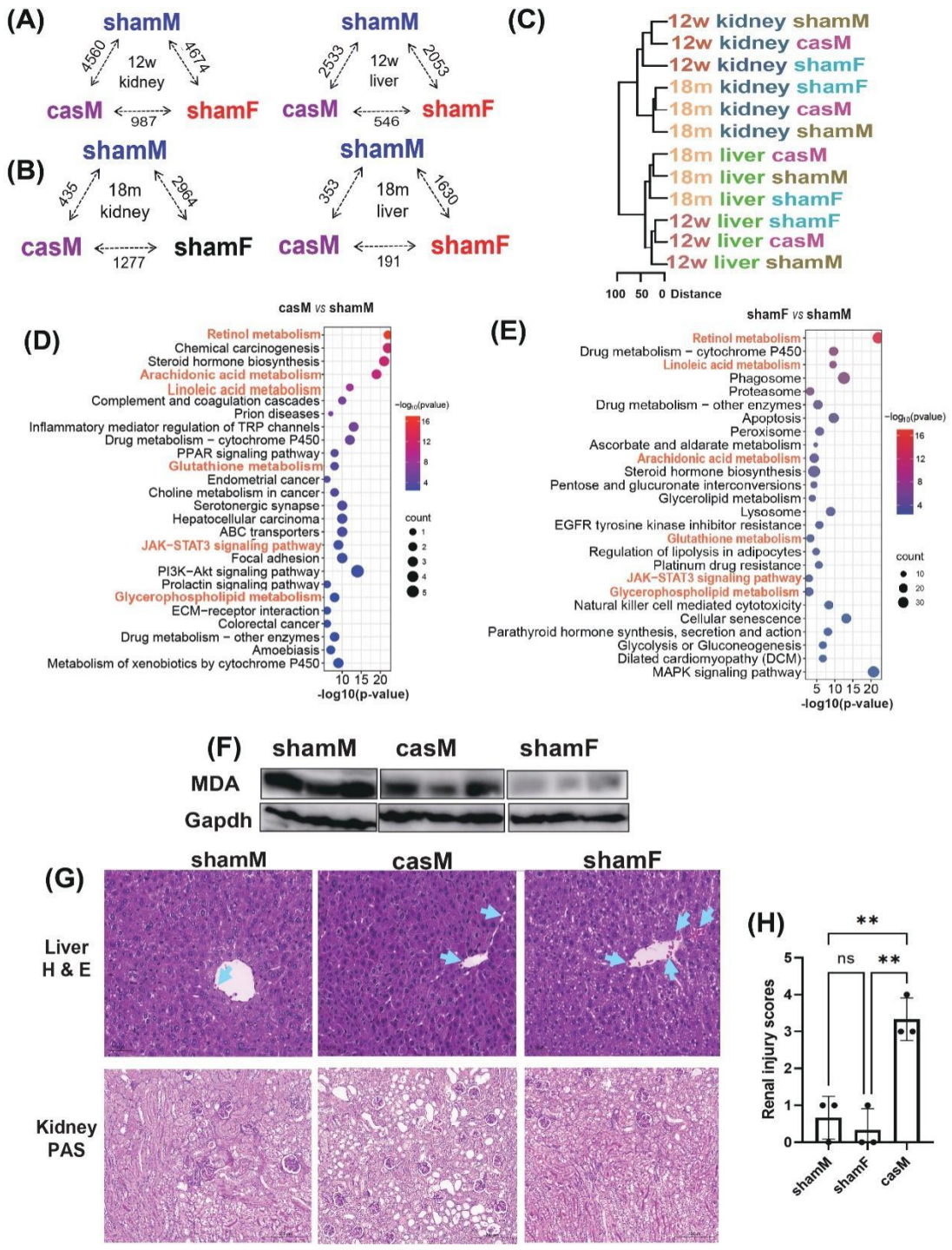

Figure 6. Joint metabolomic-transcriptomic analysis reveals a stronger capacity of defensing lipid peroxidation in female and castrated male. (**A-B**) The numbers of DEGs among livers and kidneys tissues of shamM, shamF and casM mice collected at 12w (**A**) and 18m (**B**); (**C**) Hierarchical clustering of 12w and 18m liver and kidney samples demonstrating casM's closer alignment with shamF than sham; (**D, E**) Representative significantly enriched KEGG pathways in 18m liver samples from 'casM vs ShamM,' (**D**) and 'shamF vs ShamM' (**E**), identified by joint transcriptomic-

958 metabolomic analysis using DEGs and SAMs. Pathways marked in orange indicate
959 common terms between these two comparisons. (**F**) Immunoblotting of MDA in 18m
960 livers; (**G**) H & E staining of livers (upper panel) and PAS staining of kidneys (lower
961 panel) in 12w mice (4 week post castration/sham procedure) with cisplatin treatment,
962 blue arrows indicate representative injury spots in livers; (**H**) Bar plots of renal injury
963 scores in three groups of mice by One-Way ANOVA test (**$p < 0.01$, ns: not significant).
964
965
966